Rope Coiling on a Plane

S. Amnuanpol[*]

Physics Department, Thammasat University, Klong Luang, Pathumthani 12120, Thailand

[*]E-mail: sitichok@tu.ac.th

Abstract

Feeding the elastic rope steadily from the height toward a plane with constant velocity results in the circular coiling which is a manifestation of the buckling instability. The axial compressive forces, responsible for the buckling instability, are the own weight of rope due to the gravity and the inertial force due to the momentum of rope. The coiling frequency and the coiling radius are studied as a function of height and feeding velocity. Remarkably, there exists a characteristic velocity v^* at which the coiling radius is largest. At feeding velocity faster than the characteristic velocity v^* the inertial force dominates over the gravitational force. This characteristic velocity v^* is experimentally found to increase with decreasing height h in qualitative agreement with the dimensional analysis argument which predicts the relationship $v^* \sim h^{-1}$.

Keywords: Buckling instability: Froude number: Rope coiling: Liquid rope coiling

Introduction

Elastic objects deform continuously their shapes in response to the internal and external forces. In equilibrium the resulting shape is the conformation that minimizes energy. The deformation, such as compressing, bending, and twisting, brings the system from the present conformation to the ground state conformation. One of the equilibrium shapes is a coil with two possible chiralities, either right-handed or left-handed. Under certain circumstances both right-handedness and left-handedness are equally energetically favorable and thus coexist together, for example Figure 1(a) depicting the tendril of a Thai climbing plant, Tumlung, whose the lower portion is a right-handed coil and the upper portion is a left-handed coil. The coexistence of the right handedness and the left handedness occurs when decreasing the tension slowly with both ends not allowed to rotate [1].
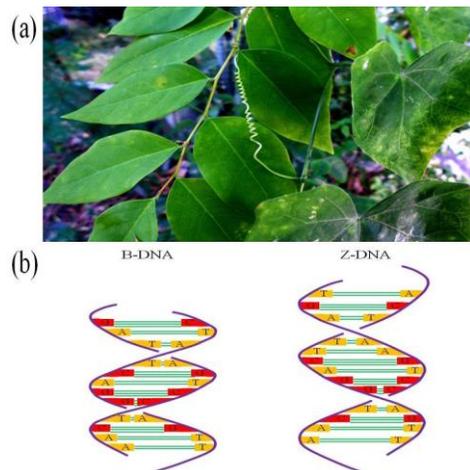

Figure 1 Right-handed and left-handed coils commonly found in nature. (a) Tendril of Tumlung winds both right-handed and left-handed directions. (b) B-DNA with 10.5 base pairs per turn is right-handed whereas Z-DNA with 12 base pairs per turn is left-handed.

On molecular level, as illustrated in Figure 1(b) the right-handed double helix, called B-DNA, is undertwisted and thus is transformed to the left-handed double helix, called Z-DNA, with identical sequence of base pairs [2].

From dynamical point of view the coiling is a consequence of buckling instability, caused by the too large amplitude bending. Such bending is created by an axial compressive stress. The down-to-earth example seen in our daily life is the coiling of the honey stream falling from the sufficient height [3]. To elucidate the general features of this phenomenon we mimic it by a well-controlled table-top experiment in which the rope is fed to a plane with constant rate and coils up repeatedly.

Materials and Methods

The 6 m long rope with radius $a_0 = 0.1\,\mathrm{cm}$ is fed from the platform toward the plane by a pulley driven by the dc motor. Its mass density ρ is $0.51\,\mathrm{g/cm^3}$. Its cross-section area A is $3.14 \times 10^{-2}\,\mathrm{cm^2}$ so the moment of inertia of the cross-section $I = A^2/2\pi$ is $1.57 \times 10^{-4}\,\mathrm{cm^4}$. The Young's modulus E is 2.43 MPa determined from the slope of the stress-strain curve. The radius a_0, cross-section area A, and the moment of inertia of the cross-section I are the geometrical properties of the rope. The mass density ρ and the Young's modulus E are the material properties of the rope. The interplay of the geometrical and material properties dictates the behavior of rope coiling. The Figure 2 shows a schematic of the experimental setup. The height h ranges from 6.5 cm to 168.5 cm. The feeding velocity of the rope $\mathbf{V}$, which is controlled by the voltage applied to a dc motor, ranges from 3 cm/s to 64 cm/s. The frequency of the pulley rotation is measured by an encoder which generates a train of 500 step functions per a turn of rotation. Knowing the frequency of the pulley rotation and the radius of pulley 6.4 cm, the feeding velocity $\mathbf{V}$ is straightforwardly calculated. Upon reaching the plane the rope coils steadily with constant frequency f. It interrupts the LED beam of the photoelectric sensor twice for each turn of coiling. Its coiling frequency f can be deduced from examining the output signal of the photoelectric sensor monitored on an oscilloscope. Its coiling radius R is measured by a vernier. The periodically varying shape of the rope is recorded by a camera.
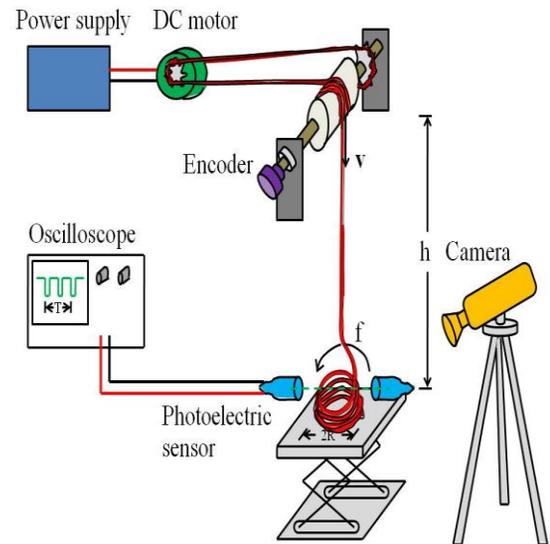

Figure 2 Experimental setup for measuring the coiling frequency f of the rope fed from the height h with uniform velocity $\mathbf{V}$.

Results and Discussion

Basically the behavior of rope coiling is determined by the interplay of three forces exerting on the rope, the elastic force F_E being the internal force due to deformation, the gravitational force F_G due to gravity, and the inertial force F_I due to the momentum of rope [4]. The latter two forces are external forces. The relative role of these three forces is quantified by three dimensionless parameters. One is the Froude number measuring the ratio of the kinetic energy to the gravitational potential energy, $Fr = v^2/gh$. The second, denoted by γ, is the ratio of the gravitational potential energy to the flexural energy, $\gamma = 2\pi\rho g h^3/EA$. The third is the slenderness measuring the rope radius to the height, $\epsilon = a_0/h$. In our experiments the Froude number Fr ranges from 6×10^{-5}, achieved at

minimum velocity 3 cm/s and maximum height 168.5 cm, to 7×10^{-1}, achieved at maximum velocity 64 cm/s and minimum height 6.5 cm. For Froude number $Fr \ll 1$ the gravitational force F_G is most dominant. Increasing the Froude number to the order of one $Fr \approx 1$, the inertial force F_I now plays as important role as the gravitational force F_G. The parameter $\hat{\gamma}$ ranges from 1, achieved at minimum height 6.5 cm, to 2×10^4, achieved at maximum height 168.5 cm. The slenderness ϵ ranges from 6×10^{-4}, achieved at maximum height 168.5 cm, to 2×10^{-2}, achieved at minimum height 6.5 cm.
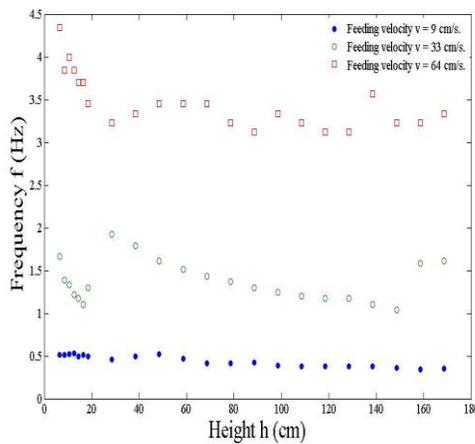

Figure 3 The height dependence of the coiling frequency is shown for feeding velocities $v = 9$ cm/s, $v = 33$ cm/s, and $v = 64$ cm/s.

As shown in Figure 3, the rope fed with the slow feeding velocity $v = 9$ cm/s coils with smaller frequency f when the height h is increased. However this trend has not persisted into the large height regime. Beyond the 100-cm height the coiling frequency f turns out to be relatively height independence, signifying the dominance of the gravitational force F_G. For intermediate feeding velocity $v = 33$ cm/s, except from the height smaller than 30 cm and from the height larger than 160 cm, the coiling frequency f decreases more rapidly with increasing height h than that in the slow feeding velocity. For fast feeding velocity

$v = 64$ cm/s the coiling frequency f also decreases with increasing height h but with the slight fluctuation. At this feeding velocity $v = 64$ cm/s, i.e. Froude number Fr being approximately of order one, the equally important roles of the gravitational force F_G and the inertial force F_I give rise to such slight fluctuation which in liquid rope coiling appears as the multiple values of coiling frequency f observed at a single height [5].
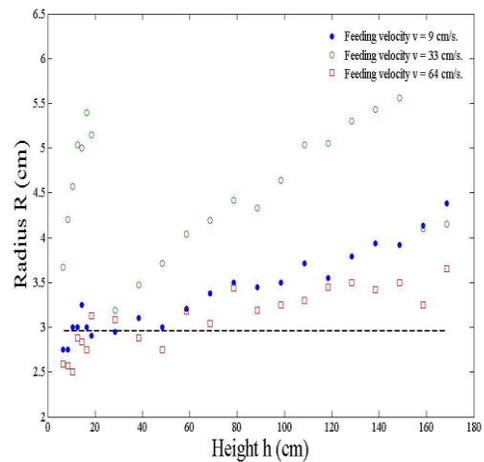

Figure 4 The height dependence of the coiling radius is shown for feeding velocities $v = 9$ cm/s, $v = 33$ cm/s, and $v = 64$ cm/s. For comparison the dash line is the radius of curvature, $(EI/\rho g a_0)^{1/4} \approx 3$ cm, created by the weight-induced bending only.

Given a value of feeding velocity v, the coiling radius R becomes bigger at large height as shown in Figure 4. However the behavior of coiling radius R looks complicated at small height less than 30 cm. The fact that increasing the height h enlarges the coiling radius R and slows down the coiling frequency f can be understood on a basis of the conservation of rope mass in order to keep $v = 2\pi f R$ constant. The horizontal dash line in Figure 4 shows the radius of curvature, created by the bending due to the own weight of rope, $(EI/\rho g a_0)^{1/4}$ which is about 3 cm for the rope we use [6]. The lower portion of the rope that lays down on the plane stops instantly, i.e. $v = 0$,

while the upper portion has still moved continuously with feeding velocity v toward the plane. This momentum change within the rope gives rise to the force $\rho A v^2$ compressing axially on the rope, creating the bending in addition to the one due to the own weight of rope. As a result the coiling radius R is overall above 3 cm, especially at feeding velocity $v = 33 \text{ cm/s}$. Increasing the feeding velocity from $v = 9 \text{ cm/s}$ to $v = 33 \text{ cm/s}$ the coiling radius R gets larger over a wide range of heights. However the further increase in the feeding velocity from $v = 33 \text{ cm/s}$ to $v = 64 \text{ cm/s}$ turns out to narrow the coiling radius R. This suggests that there exists a characteristic velocity v^* across which the behavior of coiling radius R changes qualitatively.
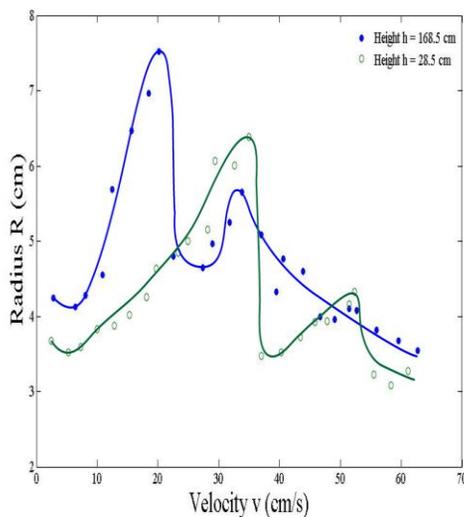

Figure 5 The velocity dependence of the coiling radius is shown for height $h = 168.5 \text{ cm}$ and $h = 28.5 \text{ cm}$. The solid lines are guide to eyes. In the large feeding velocity regime the decrease of coiling radius with increasing height signifies the dominance of the inertial force F_I over the gravitational force F_G.

Given a value of height h, shown in Figure 5, the coiling radius R increases with feeding velocity v and reaches a maximum at the characteristic velocity $v^* \approx 20 \text{ cm/s}$ for height 168.5 cm, and $v^* \approx 35 \text{ cm/s}$ for height 28.5 cm. The further increase in feeding velocity v beyond the characteristic velocity v^* turns out to make the coiling radius R smaller. This qualitative change in the behavior of coiling radius R, when crossing the characteristic velocity v^*, is attributed to a fact that at large feeding velocity the inertial force F_I becomes more important. As the height h smaller, the characteristic velocity v^* is shifted to the larger value, delaying the inertial force F_I to play the major role. This finding can intuitively be understood on a basis that the rope fed from the smaller height has the shorter length measured from the point of contact to the feeding point, thus it is more difficult to be buckled, namely the stronger force required to bend the rope. In addition to the own weight of rope, the compressive force $\rho A v^2$ that leads to the buckling instability is provided by feeding velocity v. To buckle the rope fed from the smaller height, the required stronger force is achieved by the faster feeding velocity v, explaining why the characteristic velocity v^* increases with decreasing height h. This conceptually appealing explanation can be described in a more quantitative way. To determine the characteristic velocity v^*, balancing the elastic force $E(2a_0)^4/R^3$ with the inertial force $\rho (2a_0)^2 v^2/R$ yields the velocity, above which the inertial force F_I dominates, $v = (2a_0/R)\sqrt{E/\rho}$ [4]. The Figure 4 suggests us to approximate $R \approx h$, which is accurate up to a constant factor, giving an expression of the characteristic velocity $v^* = (2a_0/h)\sqrt{E/\rho}$. Substituting the values of rope radius a_0, Young's modulus E, and mass density ρ predicts theoretically the characteristic velocity $v^* \approx 8 \text{ cm/s}$ for height 168.5 cm, and $v^* \approx 49 \text{ cm/s}$ for height 28.5 cm in reasonably good agreement with the ones observed in experiments.

Conclusions

Our table-top experiments reveal the generic features of coiling of the elastic rods which are not restricted to the solid-like objects with using rope as a representative. The decrease of coiling frequency f

with increasing the height h, shown in Figure 3, is also observed in the coiling of the highly viscous silicone oil when height less than 10 cm [7]. The reason for the much smaller height range, compared to 168.5 cm for the rope coiling, is that in the case of liquid rope coiling, like silicone oil, the height scale is of order $(\nu^2/g)^{1/3} \approx 10 \text{ cm}$ for kinematic viscosity $\nu = 10^3 \text{ cm}^2/\text{s}$. In liquid rope coiling the coiling frequency f is typically $(g^2/\nu)^{1/3} \approx 10 \text{ Hz}$, for kinematic viscosity $\nu = 10^3 \text{ cm}^2/\text{s}$, which is higher than that in rope coiling.

The liquid rope coiling also exhibits an increase in coiling radius R with increasing the height h, similar to Figure 4 for the rope coiling. The difference between rope coiling and liquid rope coiling in this respect is that the latter has the extremely small coiling radius R being of order $(\nu Q/g)^{1/4} \approx 0.2 \text{ cm}$ for kinematic viscosity $\nu = 10^3 \text{ cm}^2/\text{s}$ and flow rate $Q = 2.15 \times 10^{-3} \text{ ml/s}$ [8].

In the large feeding velocity regime, i.e. $v > v^*$ and ignoring the secondary peak in Figure 5, the coiling radius decreases with increasing the feeding velocity in a power law fashion, $R \sim v^{-1}$ with exponent -1. In liquid rope coiling the coiling radius scales with the flow rate Q as $R = (\nu a_0^4/Q)^{1/3}$.[3] Since the flow rate is simply $Q = Av$, the coiling radius decreases with feeding velocity more slowly, $R \sim v^{-1/3}$ with exponent -1/3, in liquid rope coiling than in rope coiling.

The resemblance between rope coiling and liquid rope coiling may come with no surprise because they both originate from the buckling instability. For a resting plane the shape of rope coiling is perfectly circular. When the plane moves horizontally with constant velocity, such as a conveyor belt, the moving plane breaks the rotational symmetry of the circular coiling. The rope coiling bifurcates into a variety of shapes, initiating a series of shape transitions from the translated coiling, alternating loop, and eventually to the meandering as the velocity of the moving plane is increased [9]. The analogous phenomenon is also observed in the liquid rope coiling on the moving plane with one more shape emerges because of its viscous nature, namely transiting from the translated coiling, alternating loop, meandering, and finally to the catenary as the plane moves faster [10]. It is well known that as lowering temperatures the liquid transits to the solid with the breaking of both translational and rotational symmetry [11]. Despite being the out-of-equilibrium transition, the shape transition is in some ways analogous to the phase transition.

References

[1] McMillen, T. and Goriely A. (2002). Tendril Perversion in Intrinsically Curved Rods. *J. Nonlinear Sci. 12,* 241-281.

[2] Howell, M. L., Schroth, G. P. and Ho, P. S. (1996). Sequent-dependent Effects of Spermine on the Thermodynamics of the B-DNA to Z-DNA Transition. *Biochemistry, 35,* 15373-15382.

[3] Ribe, N.M., Habibi, M. and Bonn, D. (2012). Liquid Rope Coiling. *Annu. Rev. Fluid Mech., 44,* 249-266.

[4] Habibi, M., Ribe, N. M. and Bonn, D. (2007). Coiling of Elastic Ropes. *Phys. Rev. Lett., 99,* 154302-154305.

[5] Ribe, N.M. et al. (2006). Multiple Coexisting States of Liquid Rope Coiling. *J. Fluid Mech., 555,* 275-297.

[6] Pineirua, M., Adda-Bedia, M. and Moulinet, S. (2013). Spooling and Disordered Packing of Elastic Rods in Cylindrical Cavities. *EPL, 104,* 14005-14010.

[7] Maleki, M. et al. (2004). Liquid Rope Coiling on a Solid Surface. *Phys. Rev. Lett., 93*, 214502-214505.

[8] Blount, M.J. and Lister, J.R. (2011). The Asymptotic Structure of a Slender Dragged Viscous Thread. *J. Fluid Mech., 674*, 489-521.

[9] Jawed, M.K., et al. (2014). Coiling of Elastic Rods on Rigid Substrates. *Proc. Natl. Acad. Sci. USA, 111*, 14663-14668.

[10] Morris, S.W., et al. (2008). Meandering Instability of a Viscous Thread. *Phys. Rev. E, 77*, 66218-66229.

[11] Landau, L.D. and Lifshitz, E.M. (1970). Statistical Physics. Pergamon: Oxford.